

GT2009-59026

FATIGUE ANALYSIS AND LIFETIME ESTIMATION OF CENTRIFUGAL COMPRESSOR IMPELLER BLADES

Mao Yijun

School of Energy and Power Engineering

Qi Datong

School of Energy and Power Engineering

Xu Qingyu

School of Aerospace

Xi'an Jiaotong University, Xi'an, Shaanxi, 710049, P.R.China

ABSTRACT

A multistage centrifugal compressor installed in an air-separation plant was equipped with the inlet guide vanes (IGVs) at the first stage. The impeller blades of the first stage cracked when the compressor just ran about three months. A weakly coupled fluid-structure interaction (FSI) is numerically calculated to analyze the high cycle fatigue (HCF) failure and estimate the lifetime of the impeller blades. In order to obtain the time dependent aerodynamic loads on the impeller blades, three-dimensional unsteady compressible viscous flow in the first whole stage of the centrifugal compressor is simulated. And then, a data interpolation tool is developed to transfer the physical information from fluid meshes to structure meshes, and also, time dependent data is transferred into frequency dependent data using Fast Fourier Transform (FFT). The free vibration mode and forced vibration response of the impeller blades are calculated using finite element method (FEM) and the cyclic symmetry structure of the rotating impeller is modeled by a single segment. According to the numerical result, the HCF lifetime of the impeller blades is estimated using a local stress-strain method. Numerical result shows that the predominated frequency of unsteady aerodynamic loads acting on the impeller blades is equal to the frequency of the IGVs-impeller blades interaction. Both the predicted stress concentration region and lifetime of the impeller blades agree reasonably well with factual fracture case. This study shows that it is feasible to use the weakly coupled FSI simulation to predict the fracture region and lifetime of centrifugal impeller blades.

INTRODUCTION

The requirements for high reliability, high speed to turbomachines are growing, and along with the extension of operating range for energy saving. For this reasons, in order to design a more compact structure of turbomachine, the impeller vibration induced by unsteady flow becomes a very important design aspect in many cases to prevent high cycle fatigue (HCF) failures.

Impeller blade is mainly subjected to three different loads: centrifugal force, aerodynamic force and thermal stress. Centrifugal force is time-dependent when the compressor operates in an acceleration motion, such as start-up, shut down and rotational speed adjustment. But at usual operating condition with constant rotational speed, centrifugal force just only generates static stress on impeller blades. Thermal stress is an important cause that generates HCF of steam turbine blades [1], but for the centrifugal compressor, the surface temperature of impeller blade is usually not more 150°C, and thus the aerodynamic heats effects could be neglected.

Unsteady aerodynamic force is the main source that drives the centrifugal compressor impeller into destructive vibration. There exist so many causes that generate and affect unsteady aerodynamic force on impeller blades, such as potential and viscous interaction, vortex separation, secondary flow and stall flow, et al. Many researchers have contributed to understand the unsteady flow mechanism of turbomachines. The theories of unsteady aerodynamic forces in turbomachine stage are described by Rao [2]. Fast response pressure transducers are usually used to measure the unsteady pressure of discrete points on the low rotational speed impeller blades [3-5]. Recently, a more advanced porous pressure sensitive paint

(PSP) technique has been successfully applied to measure the unsteady pressure on the whole surface of rotating blade [6]. With the rapid development of computational fluid dynamics (CFD) and computer hardware, numerical studies on the three-dimensional unsteady viscous compressible flow and aerodynamic forces in centrifugal compressor have been carried out using unsteady RANS equations [7,8] and large eddy simulation [9,10].

Blade vibration induced by unsteady aerodynamic force is essentially a fluid-structure interaction (FSI) phenomenon, and many FSI models have been proposed at last years [11, 12]. Coupled simulation of nonlinear FSI on a centrifugal compressor has been done by Carstens et al [13, 14]. Experimental investigation on the compressor blade vibration has been carried out by Dickmann et al [15]. Both numerical and experimental results show that the flow-induced vibration of shrouded centrifugal impeller is a low-amplitude vibration. In engineering, the weakly coupled FSI simulation is usually adopted to analyze the forced vibration response of blades, which neglects the effect of blade vibration to unsteady flow in passage channel. Filsinger et al [16] and Misek et al [17] have used this approach to analyze the forced vibrations of axial turbomachinery turbine blades and steam turbine blades, respectively. Similar numerical studies on the blades vibration of a centrifugal compressor have been done by Dickmann et al [15] and Srivastava et al [18].

One of the most important factors for controlling the forced response of blade is the damping that exists in the system. Impeller blade damping is composed of three major sources: material damping (due to inherent material properties), structural damping (due to the frictional contacts) and aerodynamic damping (due to the motion induced unsteady pressure around the blade). Material damping is negligibly small for typical metal alloys used in the construction of blades, can be often ignored [19]. Structural damping is dependent on the rotational speed. Experimental result of Rao [20] shows that when the impeller rotates at speed higher than 1000rpm, blade root gets totally interlocked with the disk and there is no relative movement, the structural damping is even smaller than material damping. Experimental results of aerodynamic and structural damping obtained by Kielb [21] also indicate that the structural damping is inversely proportional to the square of the speed, and the aerodynamic damping is a large component of the tonal damping for all modes.

Cumulative damage theories are usually applied to estimate the blade lifetime, including linear and nonlinear models. The most of them is the linear one proposed by Miner [22], and the nonlinear theories including Corten-Dolan model considering load-sequence effect [23], Manson-Halford model based on double linear damage rule and damage curve approach [24], Niu model based on energy method [25], and etc.

In this paper, a case study on the HCF of compressor blades has been carried out using the weakly coupled FSI approach. In order to analyze the fracture cause of the impeller blades, a numerical study on the unsteady compressible viscous flow and

forced vibration in centrifugal compressor has been carried out, and the estimation of blade HCF lifetime has been performed combining Miner's linear cumulative damage theory and local stress-strain approach.

NOMENCLATURE

| | |
|-----------------------------------|--|
| b | Fatigue strength exponent |
| c | Fatigue ductility exponent |
| \mathbf{C} | Damping matrix [Kg/s] |
| dS | Cell area [m ²] |
| E | Young's modulus |
| \mathbf{K} | Stiffness matrix [kg/s ²] |
| K_f | Effective stress concentrative coefficient |
| K' | Cyclic hardening exponent |
| \mathbf{M} | Mass matrix [kg] |
| n | Impeller rotational speed [r/min] |
| n' | Cyclic hardening exponent |
| N | Cyclic times |
| $p(\omega)$ | Aerodynamic load vector per unit area [Pa] |
| r | Nodal radius [m] |
| t | Unsteady time step [s] |
| T | Sampling number for one impeller revolution |
| $u(\omega)$ | Nodal displacement vector component [m] |
| Z_2 | Number of impeller blades |
| ω | Angular frequency [Hz] |
| σ_e | Von Mises stress [Pa] |
| σ_c | Static stress generated by centrifugal force [N] |
| σ_{kl} | Amplitude of k th component of stress on l th segment [Pa] |
| φ_{kl} | Phase of k th component of stress on l th segment |
| σ_m | Mean stress [Pa] |
| σ | Total alternating stress [Pa] |
| $\sigma_x, \sigma_y, \sigma_z$ | Normal stress [Pa] |
| σ'_f | Fatigue strength coefficient |
| $\Delta\sigma_n$ | Nominal dynamic stress [Pa] |
| $\Delta\sigma$ | True stress range [Pa] |
| $\Delta\varepsilon$ | True strain range |
| $\tau_{xy}, \tau_{yz}, \tau_{xz}$ | Shear stress [Pa] |
| ε'_f | Fatigue ductility coefficient |

FAILURE DESCRIPTION OF IMPELLER BLADES

The multistage centrifugal air compressor was installed in an air-separation unit, and the first stage is composed of radial induction chamber, inlet guide vanes (IGVs), impeller, vaneless diffuser, crossover and return channel vanes. Schematic of the first stage aero components is shown in Figure 1. Before indraft

into the centrifugal impeller, air flowed through the radial induction chamber and IGVs to form a pre-whirl flow. The main geometrical parameters and material properties of the first stage of the compressor are listed in Table 1. For the usual operating condition, the centrifugal compressor operated at the constant rotational speed 4995r/min, the corresponding volume flow rate was 100445m³/h.

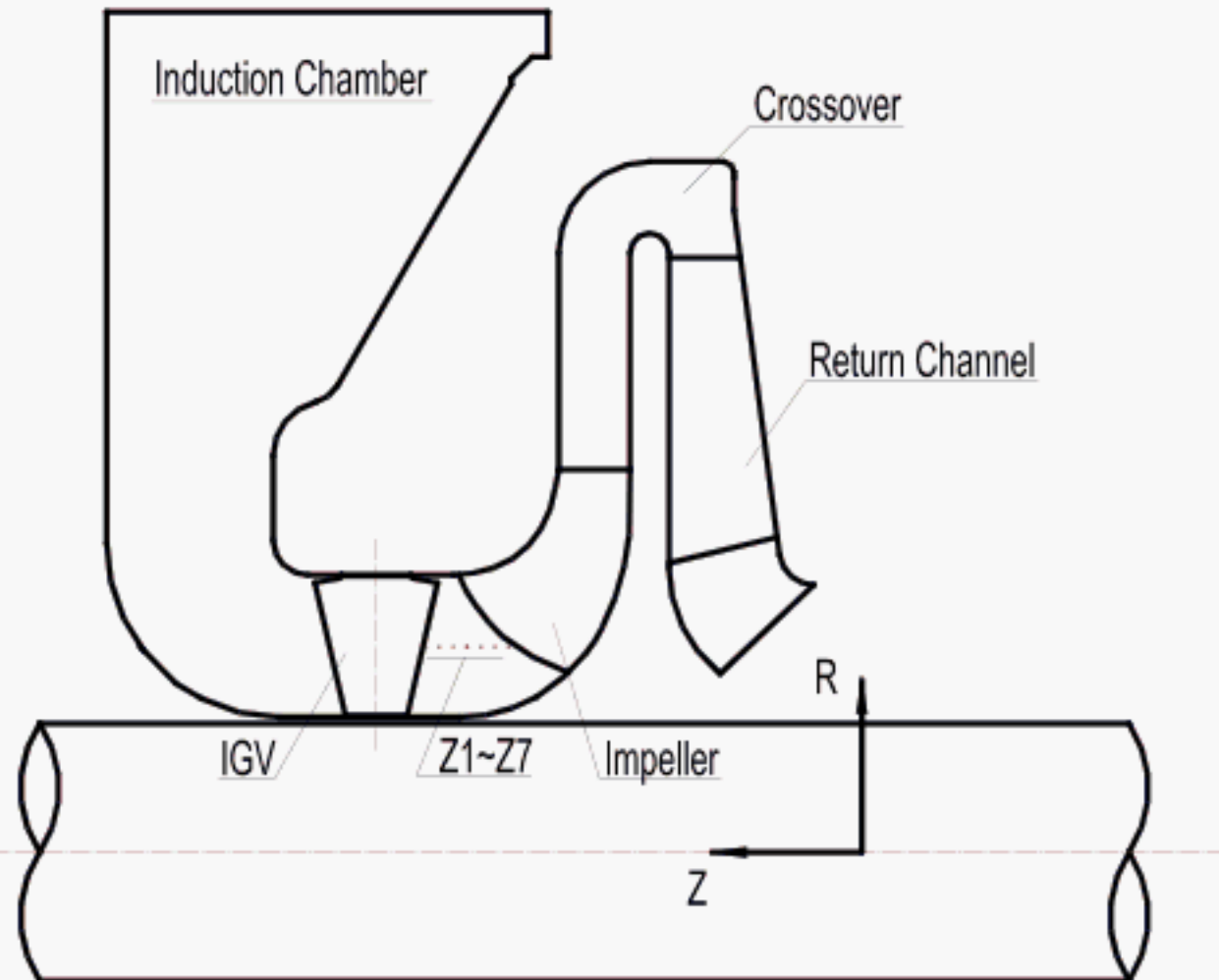


Figure 1. Main components of centrifugal compressor stage

Table 1. Geometrical parameters of first stage of the centrifugal compressor

| | |
|---------------------------------|--------|
| Number of inlet guide vanes | 14 |
| Number of impeller blades | 19 |
| Number of return channel vanes | 18 |
| Inlet diameter of hub | 386mm |
| Inlet diameter of shroud | 800mm |
| Outlet diameter of the impeller | 1100mm |

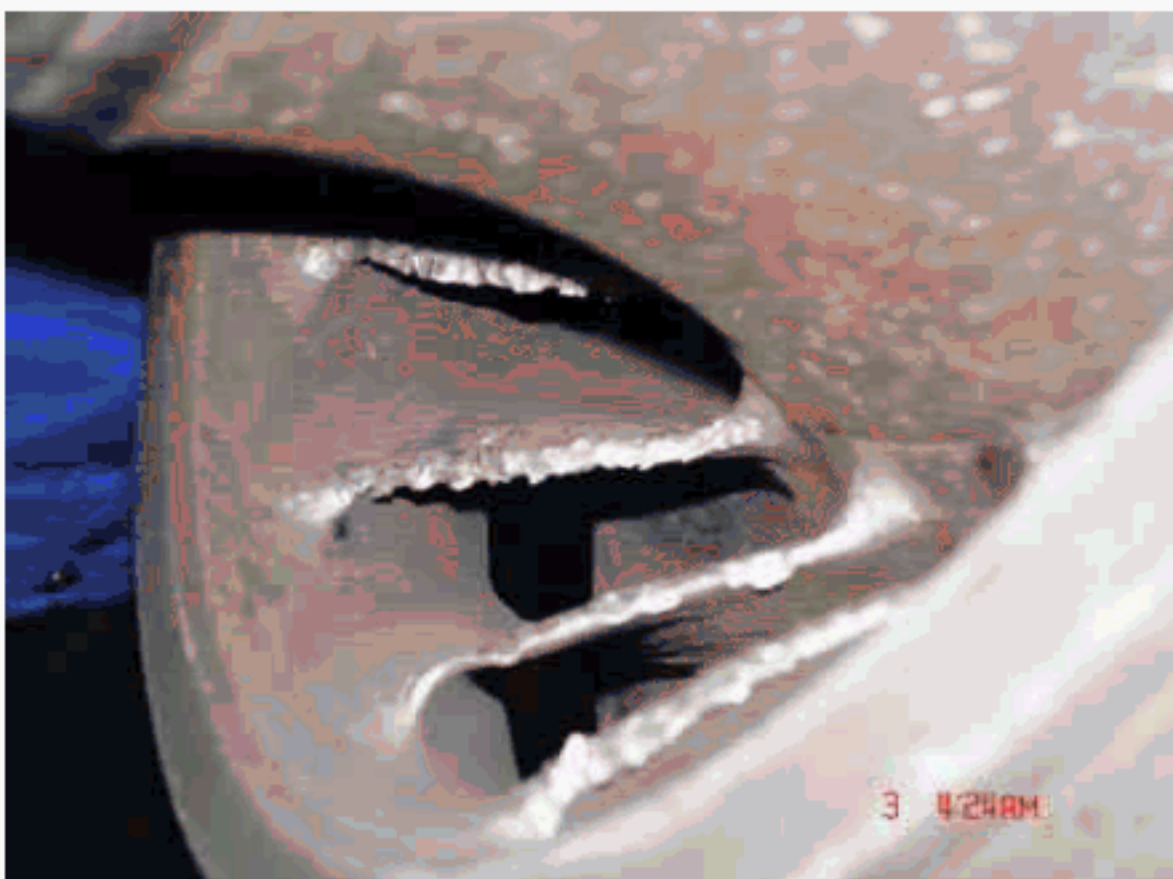


Figure 2. Photo of the cracked centrifugal impeller

The impeller blades of the first stage cracked when the compressor just ran about three months, and the fracture region was in the vicinity of leading edge of the impeller blades, as shown in Figure 2. There is non-obvious plastic deformation on the broken section of the blades. Runtime is long enough to exclude the possibility of the failure due to shaft resonance vibration. Slight corrosion of purified air in two month is impossible to crack the blades. The centrifugal compressor impeller blades don't operate at a very high temperature, and thus aerodynamic heats effects could be neglected. The most possible cause is the HCF fatigue that induced by unsteady aerodynamic forces acting on the impeller blades.

NUMERICAL MODEL

Unsteady flow simulation

Numerical calculation of the unsteady flow has been performed with a commercial software package, FLUENT. The continuity equation and Reynolds-averaged Navier-Stokes equations (RANS) for unsteady compressible viscous flow are solved in this work. Governing equations and standard k-epsilon turbulence model are discretized with finite volume method (FVM). The density-based explicit solver is adopted for unsteady compressible flows. The discretization scheme of the time-dependent term is second order, implicit. The second order upwind scheme is used for the convection and diffusion terms in order to eliminate the false diffusion error.

The complete flow passages model of first stage is adopted for the following two reasons. Firstly, the distorted flow at the inlet of IGVs caused by the radial induction chamber is not circumferentially uniform. Secondly, as the numbers of the IGVs and impeller blades are relatively prime, a single flow passage and partial flow passages model couldn't reveal the IGV-impeller interaction frequency. A complete model results in an obvious increase of numerical complexity and runtime, so we execute the CFD code on a parallel platform.

A geometrical discretization of the first stage model is made for the numerical treatment. The geometric model is divided into three unattached flow zones: inlet flow zone (induction chamber and IGV), impeller zone and outlet flow zone (vaneless diffuser, crossover and return channel vanes). Hybrid cells combined by unstructured tetrahedral cells and structured hexahedral cells are generated to define the flow zones (1,233,074 cells at total). In the impeller, the meshes around the blades are refined to calculate the unsteady aerodynamic loads.

Surfaces between IGV-impeller and impeller-vaneless diffuser are defined as the grid interfaces needed for the relative rotation of the impeller. The mixing plane approach and sliding mesh technique provided by FLUENT allow information transformation between upstream and downstream interface during the steady and unsteady flow simulation, respectively. Grid interfaces need not be matching on both sides, as an interpolating routine is defined.

The appropriate boundary conditions are those considered with more physical meaning for turbomachinery flow simulations, that is, the total pressure, total temperature, turbulent intensity, turbulent viscosity ratio, and a reference pressure at the inlet boundary of the compressor are specified. In this work, since no experimental data are available for the inlet and outlet flow. It is assumed that the inlet total pressure and total temperature are uniform in each grid node, being equal to atmosphere pressure and ambient total temperature, respectively. The turbulence intensity is assumed to be 5%, and furthermore, the turbulent viscosity ratio is assumed to be five. At the outlet boundary of the computational domain, the flow is unsteady and non-uniform, the target mass flow rate is specified and the pressure at the outlet boundary is adjusted at every iteration in order to achieve the target mass flow rate. The outlet backflow turbulent intensity is assumed to be 10% and backflow turbulent viscosity ratio is assumed to be 10. All wall boundary conditions are regarded as no-slip and adiabatic conditions. The rigid wall boundary condition of the impeller blades is assumed ignoring the effect of the blade vibration to the unsteady flow, which is a reasonable approximation because the stiffness is usually high for the shrouded centrifugal impeller with short blades.

In the two grid interfaces between the stationary and moving mesh, IGV-impeller and impeller-vaneless diffuser, the overlapping faces in the interface zones are determined at each new time step. Fluxes across each grid interface are calculated proportionally to the areas of the superposed faces.

The unsteady time step of the time-resolved CFD plays an important role in frequency analysis. The unsteady time step t is calculated with the following formula.

$$t=60/ (n \times Z_2 \times T) \quad (1)$$

where Z_2 is the number of impeller blades, n is the rotational speed of impeller. T denotes the sampling number when the impeller rotates for one flow passage, which is specified as 10. Calculated unsteady time step is 6.322×10^{-5} s, and the corresponding sampling frequency is 15817.5Hz. The top frequency of pressure fluctuation could be analyzed is about 6000Hz according to the sampling theorem, which is high enough to analyze the frequency of pressure fluctuation on the blades.

The number of iterations is adjusted to reduce the residual to an acceptable value in each time step, that is to say, the ratio between the sum of the residuals on all grid nodes and the sum of the fluxes for a given variables, such as mass flow rate, velocity component in three directions, turbulence kinetic energy and turbulent dissipation rate, is reduced to the value of 10^{-3} . Initializing the unsteady flow calculation with the steady flow solution, over ten impeller revolutions are necessary to achieve the periodic unsteady solution.

Free and forced vibration

Finite element analysis (FEA) is performed to obtain the impeller blade free vibration and forced vibration behavior.

Three-dimensional model is adopted for the calculation using the commercial code MSC.Nastran.

The equation of motion for the rotating blades can be expressed in frequency domain as follows

$$(-\omega^2 \mathbf{M} + j\omega \mathbf{C} + \mathbf{K})\mathbf{u}(\mathbf{y}, \omega) = \mathbf{M} \omega^2 \mathbf{r} + \int_S \mathbf{p}(\mathbf{y}, \omega) dS(\mathbf{y}) \quad (2)$$

where \mathbf{M} is the mass matrix, \mathbf{C} is the damping matrix and \mathbf{K} is the stiffness matrix, $\mathbf{u}(\mathbf{y}, \omega)$ is the nodal displacement vector, ω is the angular velocity and \mathbf{r} is the nodal distance to shaft center, $\mathbf{p}(\mathbf{y}, \omega)$ is aerodynamic load vector per unit area and $S(\mathbf{y})$ is the area of each cell on the blade.

The dynamic stresses on the impeller blades are computed based on the fourth strength theory. The von Mises or equivalent stress, σ_e is computed using

$$\sigma_e = \sqrt{\frac{1}{2}[(\sigma_x - \sigma_y)^2 + (\sigma_y - \sigma_z)^2 + (\sigma_z - \sigma_x)^2 + 6(\tau_{xy}^2 + \tau_{yz}^2 + \tau_{zx}^2)]} \quad (3)$$

As the centrifugal compressor operates at constant speed, so the damping ratio is assumed to be 1% according to the experimental result of Vyas and Rao [26].

The impeller is a rotationally periodic structure with 19 identical blades, while the transient aerodynamic loads on each blade are different because of the IGV-impeller unsteady interaction. Strictly speaking, the cyclic symmetry theory couldn't be applied. But our interest is the vibration mode and alternating stress of the impeller blades, the amplitudes of unsteady aerodynamic loads are the same and the phase difference is the constant for the neighboring blades, so in order to save the computation cost, we adopt the cyclic symmetry structure for the numerical analysis all the same. A single sector model is used for the finite element analysis and the model is meshed into 33 808 tetrahedral elements and 8 039 nodes.

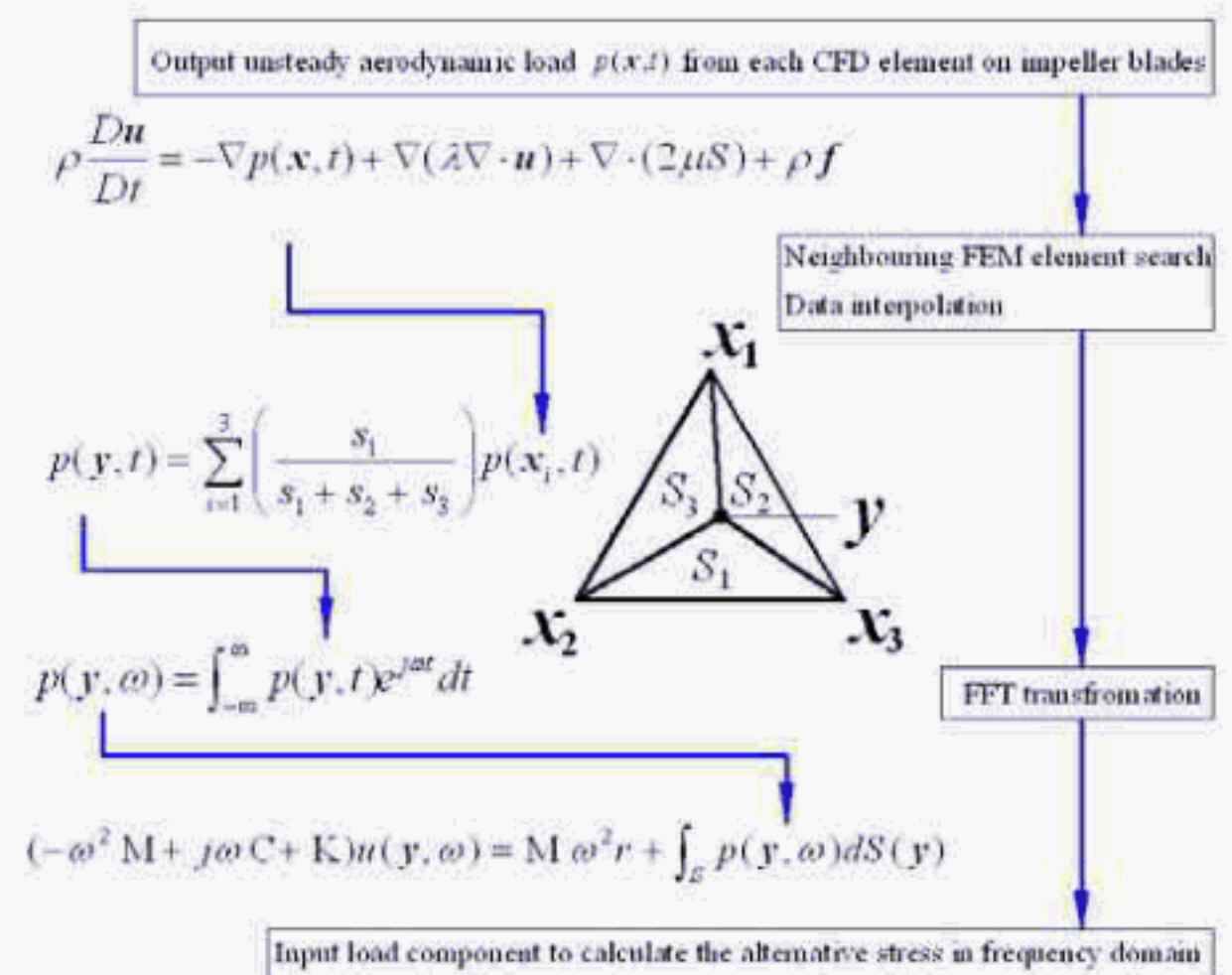


Figure 3. Flow diagram of data interpolation code

Data interpolation

The unsteady aerodynamic loads acting on each CFD node of the impeller blades are obtained from the flow simulation. There are two pieces of pretreatment works should be performed before the weakly coupled FSI simulation. Firstly, the unsteady aerodynamic loads on the CFD grid nodes should be interpolated into the FEM grid nodes. Secondly, since the time-domain structural finite element simulation needs excessive calculation time and memory, it is recommended that the analysis be performed in the frequency domain. The time-dependent pressure fluctuations on the impeller blade are transformed into the frequency-dependent signals. The data interpolation and fast Fourier transformation (FFT) programs are accomplished with the mathematic tool MATLAB. Figure 3 outlines the process of data interpolation.

RESULTS

Unsteady pressure on impeller blades

Many different types of unsteady flow in compressor might excite the pressure fluctuation on blades, such as potential flow and viscous wake flow interaction between IGV and impeller, vortex shedding from IGV and impeller blades, turbulence and secondary flow in the flow passage of the impeller, etc. The frequency features of pressure fluctuations on impeller blades induced by different flow mechanisms are list in Table 3.

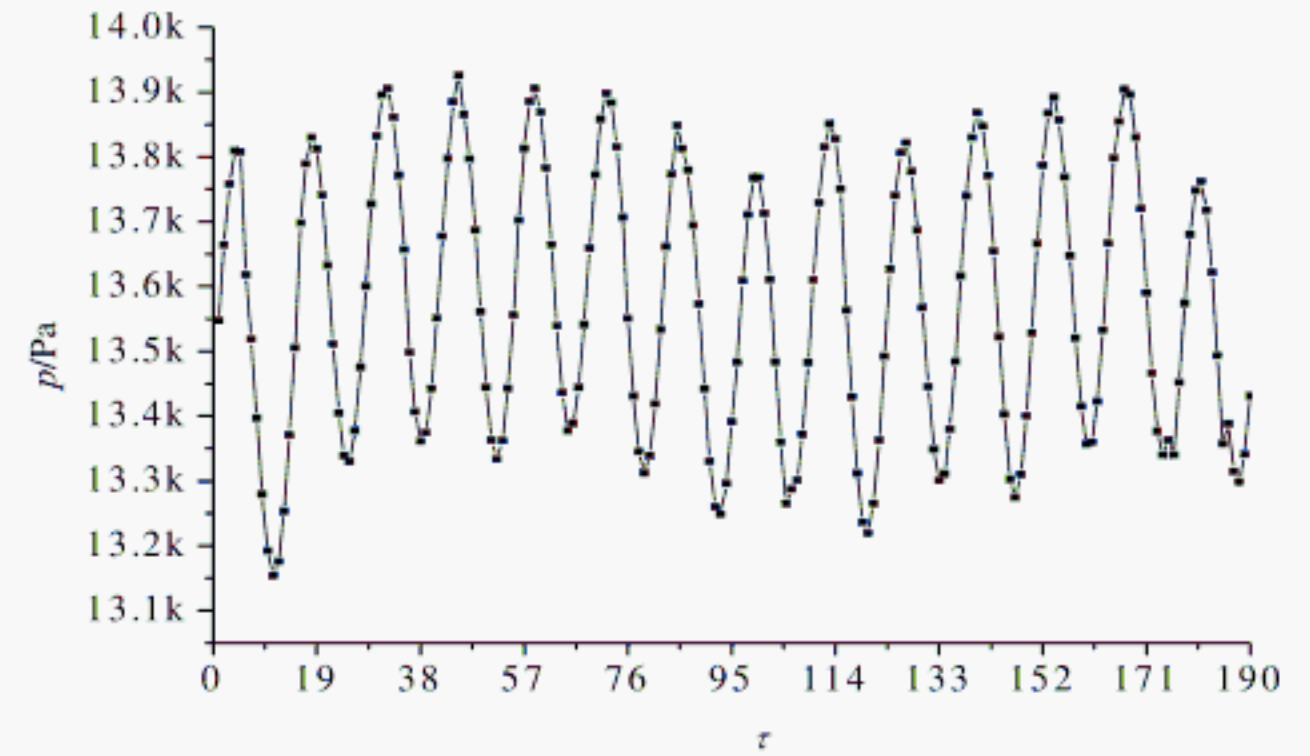
Table 3. Frequency features of unsteady pressure on blades

| No | Frequency Name | Formula | Value(Hz) |
|----|---|---|-----------|
| 1 | IGV-impeller interaction frequency f_1 | $f_1=nZ_1/60$ | 1165.5 |
| 2 | Impeller blade passing frequency f_2 | $f_2=nZ_2/60$ | 1581 |
| 3 | Vortex shedding frequency from IGV f_3 | $f_3=St \times U_1/(L_1 \sin \alpha_1)$ | (20~50) |
| 4 | Impeller rotation frequency f_4 | $f_4=n/60$ | 83.25 |
| 5 | Turbulence and secondary vortex frequency f_5 | $f_{5min} \sim O(u/D)$ | $O(10^2)$ |

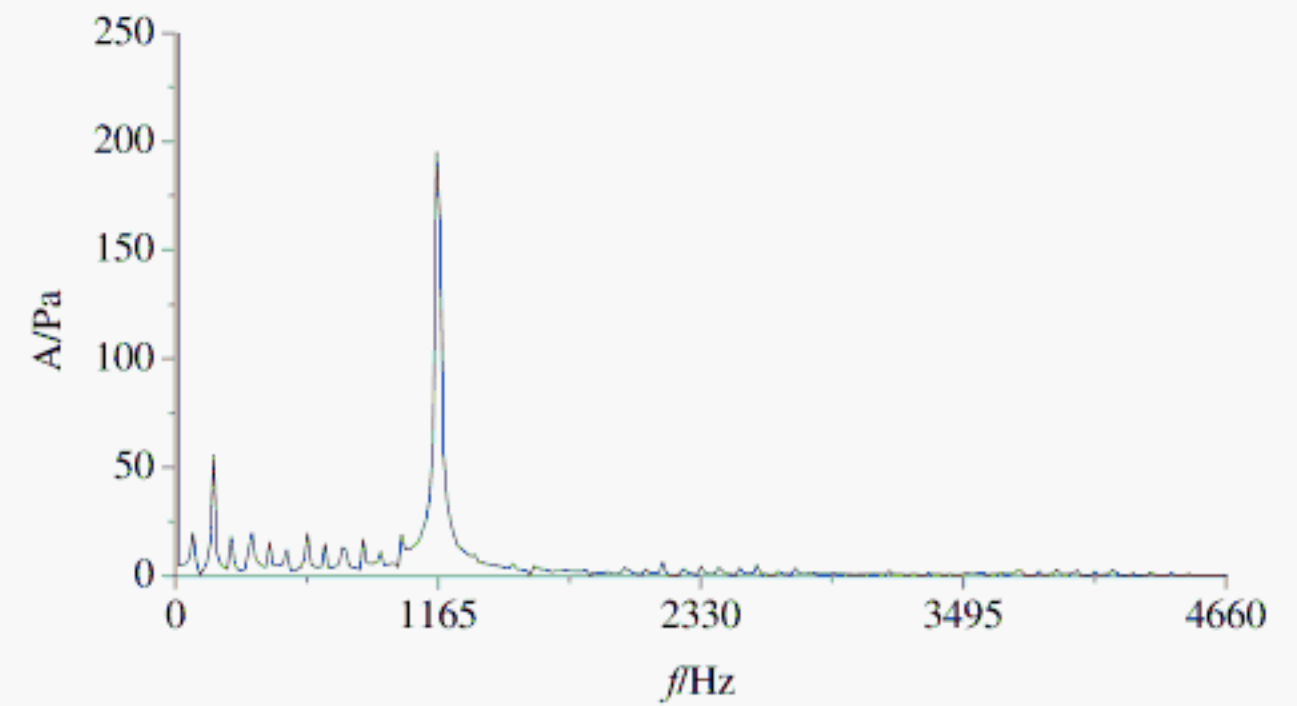
where L_1 denotes the characteristic chord length of IGV, U_1 and α_1 denote the flow velocity and attack angle at IGV inlet, u and D represent velocity fluctuation and characteristic length of turbulence in the impeller, respectively, $D=\min\{(D_0-d)/2, 2\pi D_2/Z_2\}$, S_t represents the Strouhal number, which is approximately equal to 0.15~0.30 when flow Reynolds number is above 1000[27].

The CFD calculation reveals the pressure fluctuation on the impeller blades. The pressure fluctuation of a sample point on the pressure surface is shown in Figure 4. The periodicity of pressure fluctuation during one impeller revolution is equal to the number of IGV, and the predominant frequency of pressure fluctuation is equal to fundamental frequency of IGV-impeller interaction. Further study shows the predominant frequencies

of the pressure fluctuations on both pressure surface and suction surface are equal to IGV-impeller interaction frequency, but the peak values are variable at different locations. The peak values of pressure fluctuations component at fundamental frequency on the pressure surface and suction surface are shown in Figure 5(a) and 5(b), respectively. The pressure fluctuation amplitude near the leading edge of the impeller blade is much higher than that at the other location.

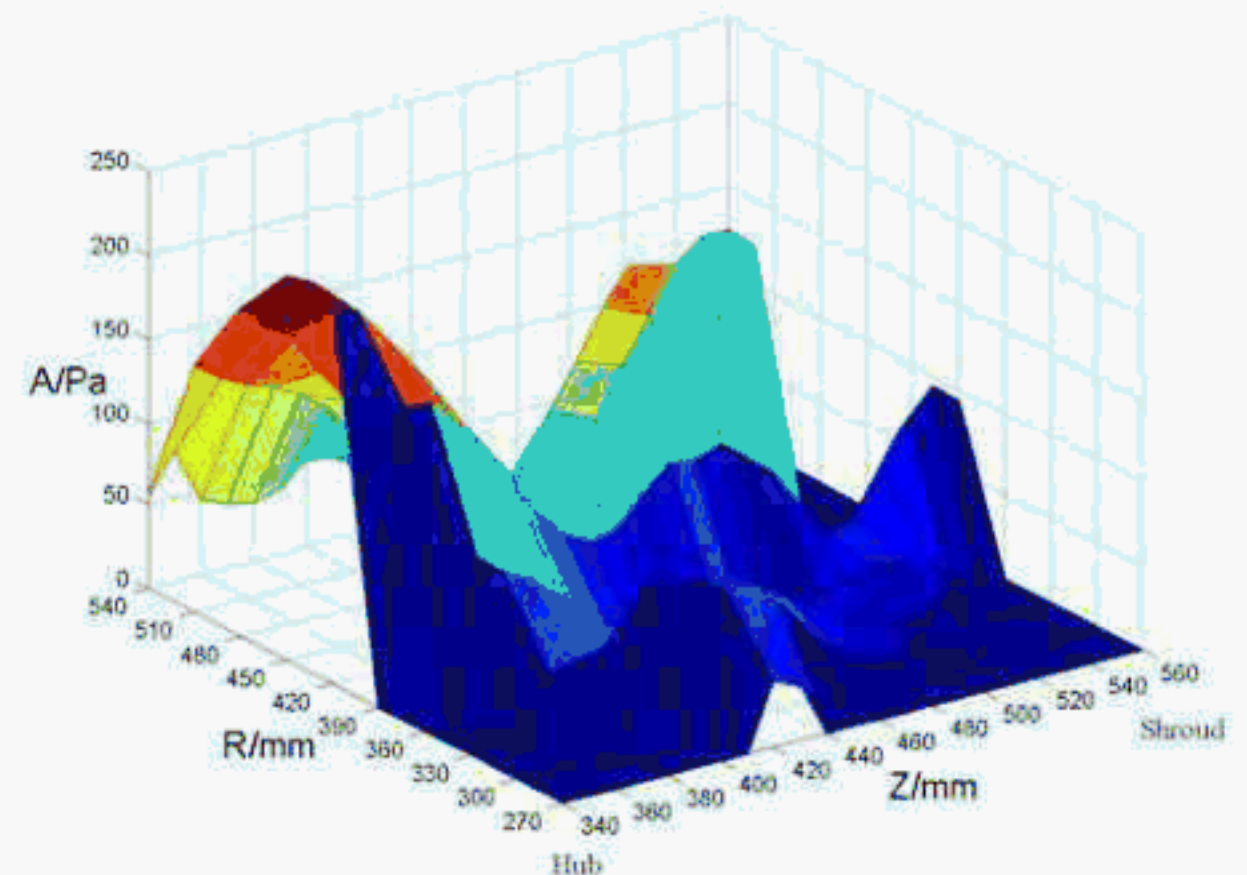


(a) Pressure fluctuations for one rotation of the impeller

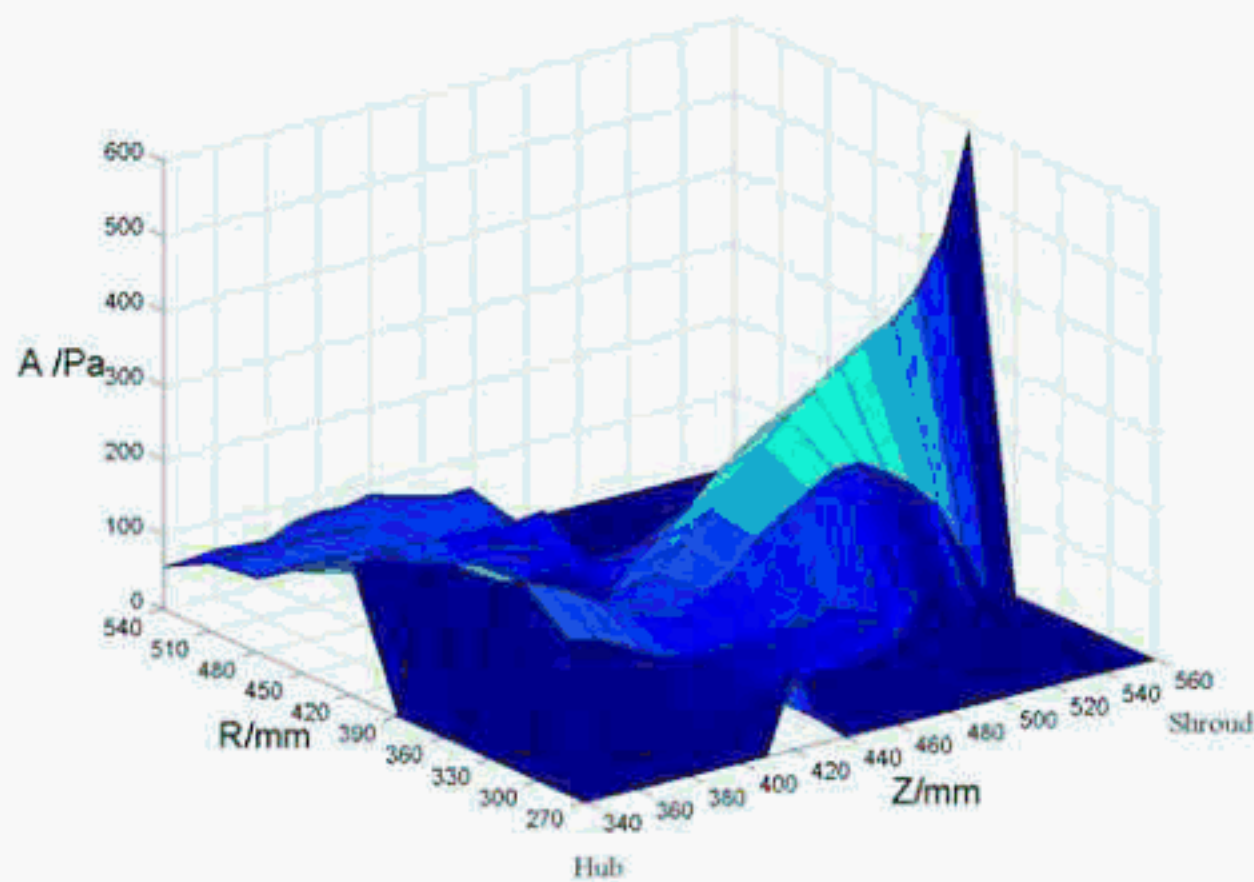


(b) Pressure spectrum

Figure 4. Unsteady pressures on the pressure surface of impeller blade



(a) Pressure surface



(b) Suction surface

Figure 5. Peak value of pressure fluctuation on impeller blade

IGV-impeller blades interaction

The absolute velocity contour between IGV and impeller blades is shown in Figure 6. An obviously viscous wake flow occurs near the trailing edge of the IGV, where the velocity is much less than the mean flow velocity. A valley of pressure fluctuation generates on the blade surface when impeller blade passes through the viscous flow wake region.

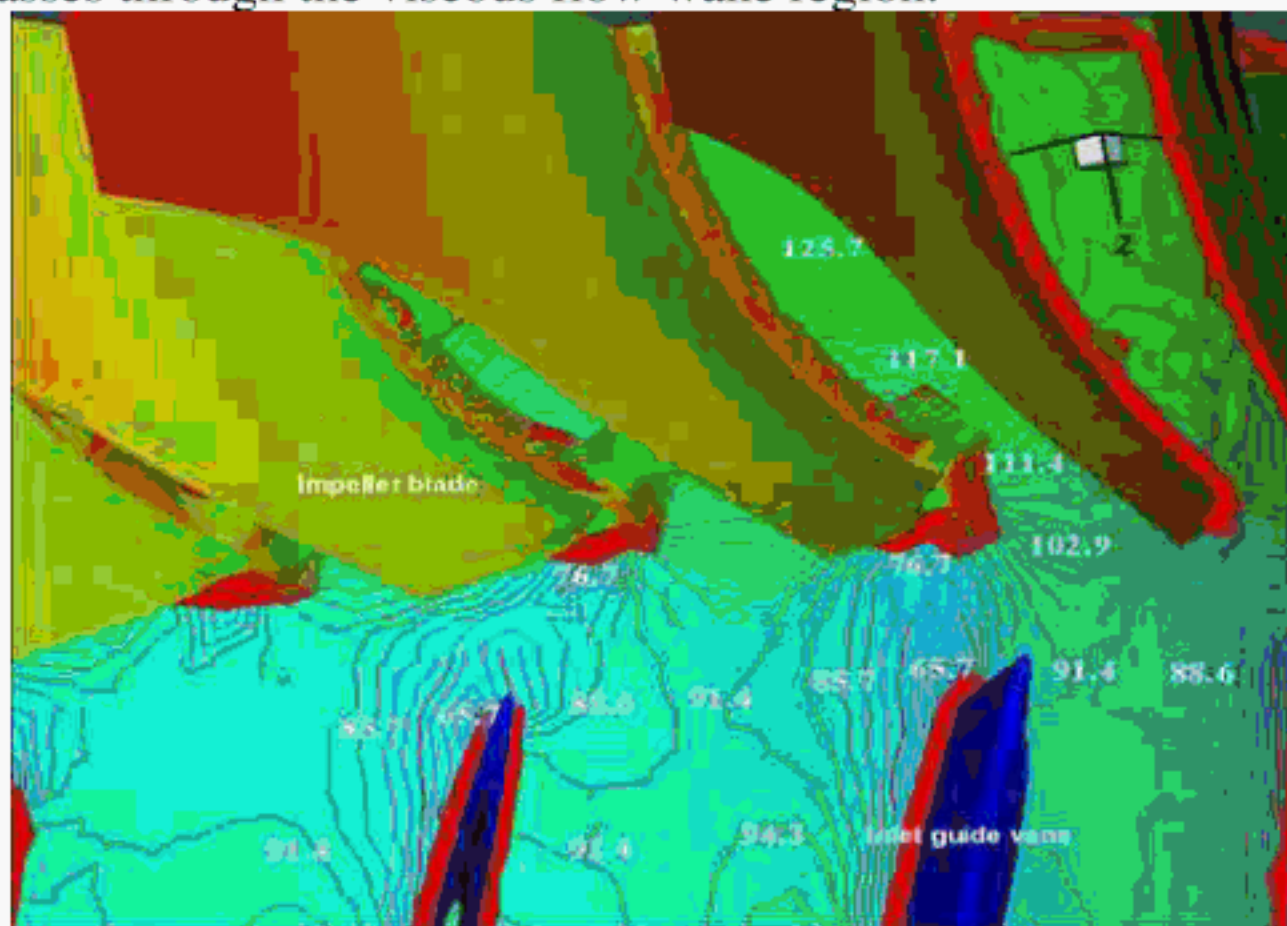


Figure 6. Velocity contour between IGV and Impeller

Circumferential distribution of static pressures at different axial positions between IGV and impeller are shown in Figure 7. Since the number of pressure peaks near the trailing edge of IGV and leading edge of impeller blades are equal to the number of IGV and impeller blades, respectively, it is thought to be caused by relative motion between IGV and impeller, that is, the effect of the potential interaction. The potential interaction is found to be dominant near the trailing edge of

IGV and leading edge of impeller blades because the pressure peak depresses far from the IGV and impeller blades.

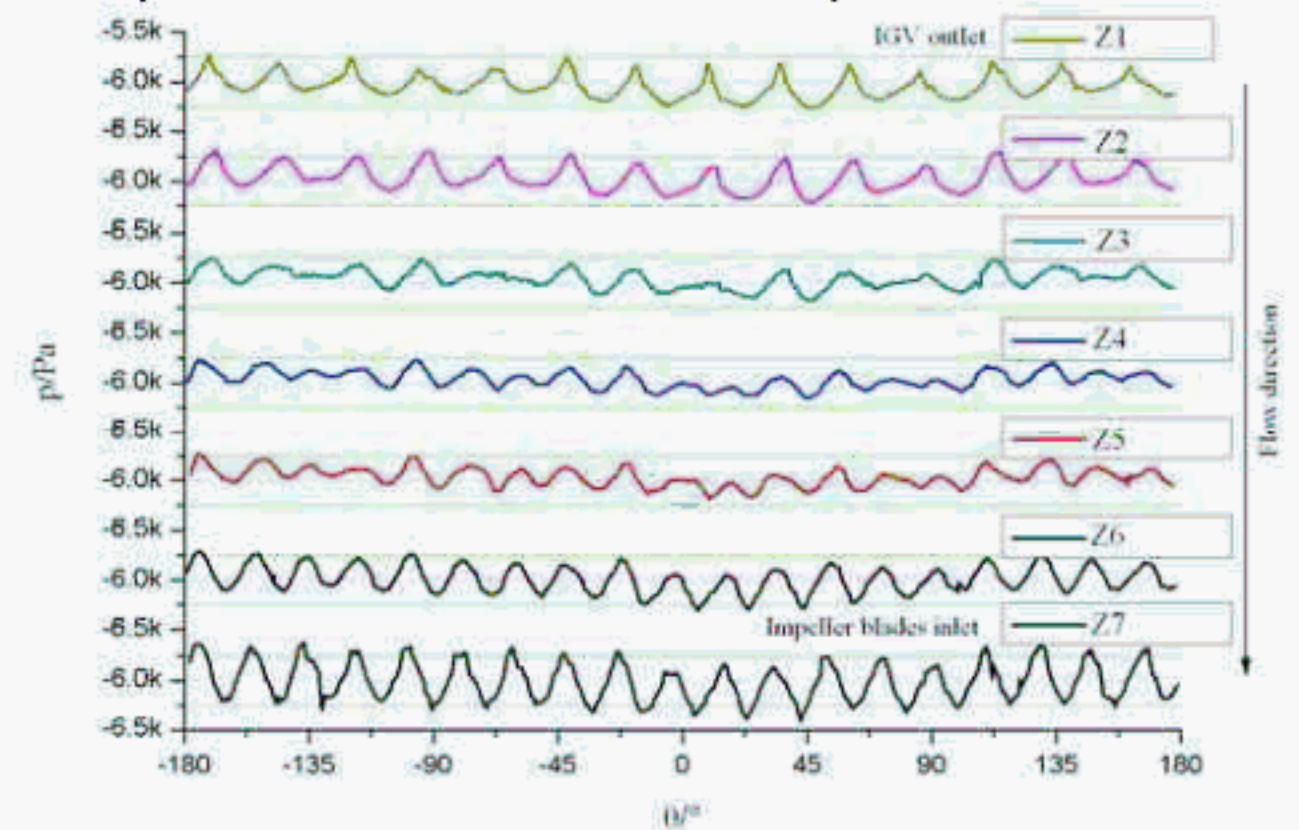


Figure 7. Pressure circumferential distribution between IGV outlet and impeller inlet

Above analysis indicates that both unsteady potential flow and viscous wake flow interaction between IGV and impeller are dominant factors that affect the pressure fluctuation on the impeller blades.

Free vibration mode and frequency margin

Neglecting damping effects, the free vibration of single sector is analyzed. The 1st-14th natural frequencies and frequency margins to the fundamental frequency are listed in Table 4. The frequency margin M% is calculated with following formula

$$M\% = |f_N - f_1| / f_1 \times 100\% \quad (4)$$

where f_N is the Nth natural frequency of the impeller blade, f_1 is the IGV-impeller interaction frequency. In engineering, the required frequency margin as an in-house rule should be more than 20% [28].

Table 4. Natural frequencies and frequency margins of the single blade

| | | | | |
|----------|--------|--------|--------|--------|
| Mode | 1st | 2nd | 3rd | 4th |
| f/Hz | 532.9 | 594.2 | 620.8 | 972.8 |
| Margin % | 118.7 | 96.1 | 87.7 | 19.8 |
| Mode | 5th | 6th | 7th | 8th |
| f/Hz | 994.7 | 1284.4 | 1309.2 | 1415 |
| Margin % | 17.2 | 9.3 | 11.0 | 17.6 |
| Mode | 9th | 10th | 11th | 12th |
| f/Hz | 1446.3 | 1453.8 | 1476.2 | 1489.9 |
| Margin % | 19.4 | 19.8 | 21.0 | 21.8 |

As the 4th-10th frequency margins are less than the required value, a local resonance on the blade will occur on the excitation of unsteady aerodynamic loads. Frequency margin between the 6th natural frequency and fundamental frequency of pressure fluctuation is the least. The 6th mode shape of the single sector is shown in Figure 8, which denotes a local vibration at the leading edge of the impeller blade. It can be

deduced that vibration amplitude near the leading edge of the impeller blade is larger than that at the other positions and stands a good chance to cause the blade HCF failure.

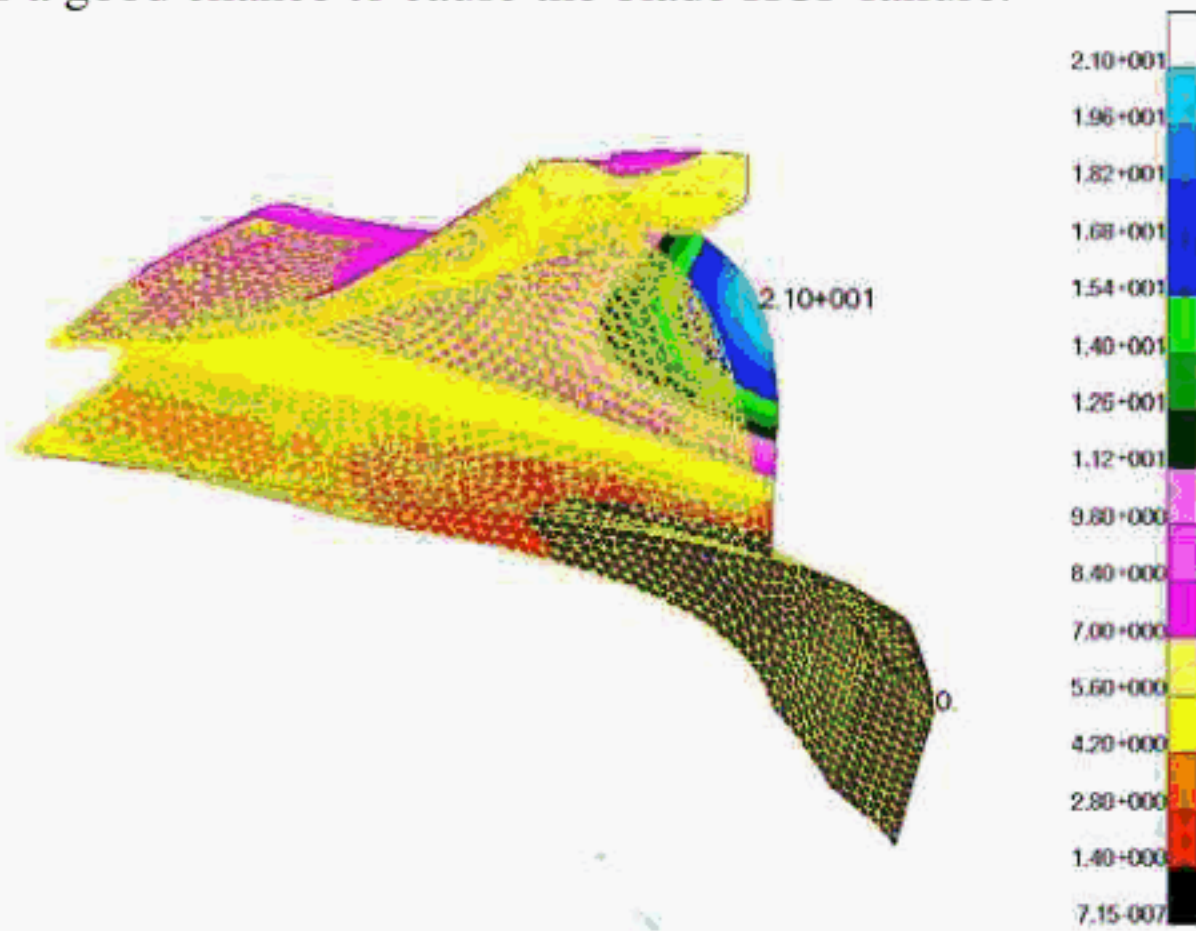


Figure 8. The 6th mode shape of impeller blade

Static stress

The impeller rotates with a high speed and centrifugal force is the primary source that generates the static stress on the blades. As shown in Figure 9, the maximum equivalent static stress on the impeller blade is 651MPa, which is lower than the yield stress 736MPa. The fracture failure of impeller could not occur just only due to centrifugal force.

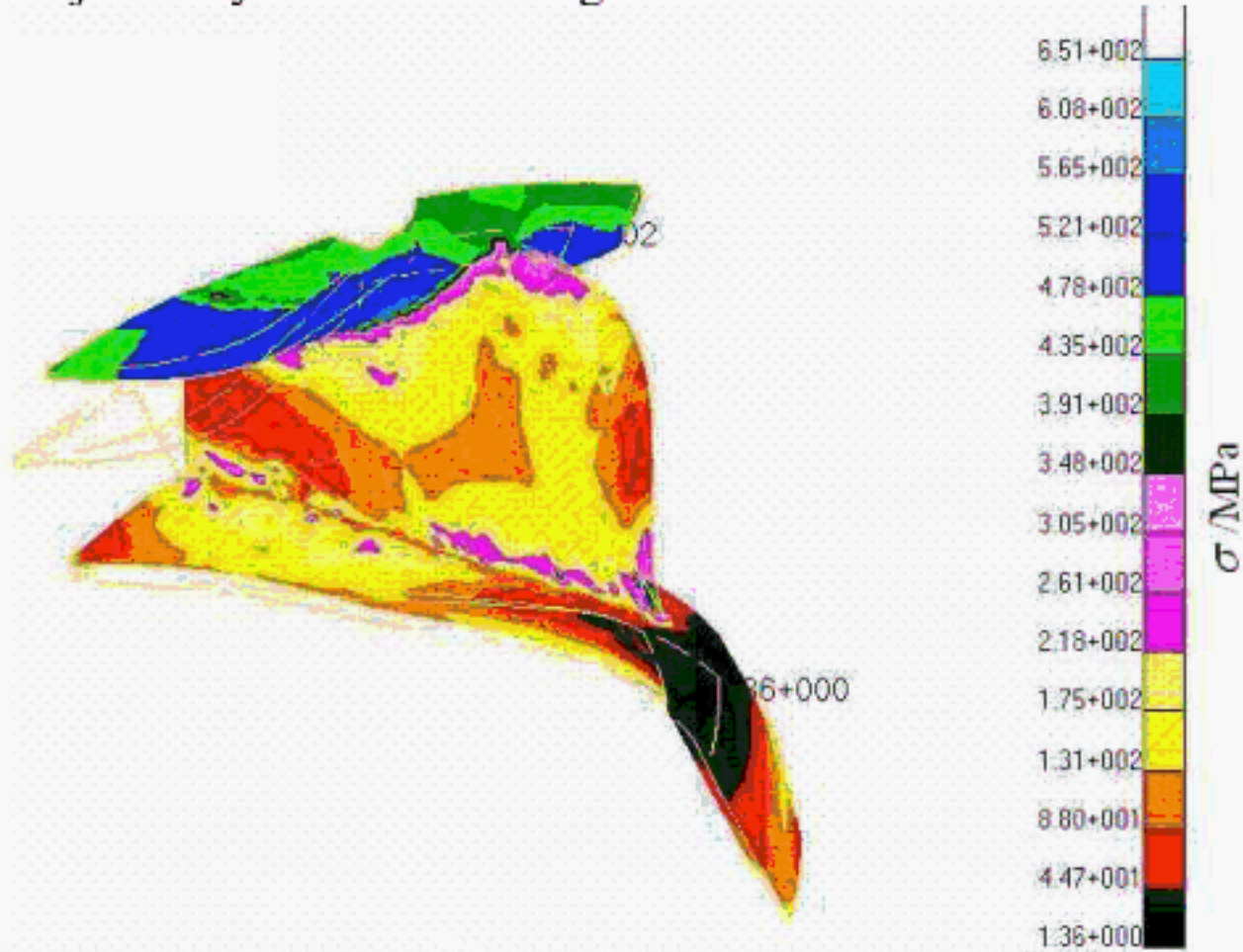


Figure 9. Static stress on impeller blade

Alternating stress

In order to consider the effect of unsteady aerodynamic load to the blade vibration, the forced response is analyzed with direct frequency method. The equivalent alternating stress induced by the fundamental frequency component of unsteady aerodynamic load is shown in Figure 10. Unsteady aerodynamic load induces a local resonance vibration and generates an alternating stress concentration region near the leading edge of impeller blade.

Although the stress at the leading edge of the impeller blade is higher than that at the other locations, the maximum stress is just only 1.35×10^{-2} MPa. The equivalent stress is much lower than the yield stress, the plastic failure (low cycle fatigue) of the impeller couldn't occur. It can be deduced that the type of the impeller crack is a HCF failure. The blade HCF failure is caused by the long-term excitation of small amplitude, low energy and unsteady pressure. The predicted high stress region is consistent with the actual fracture failure location.

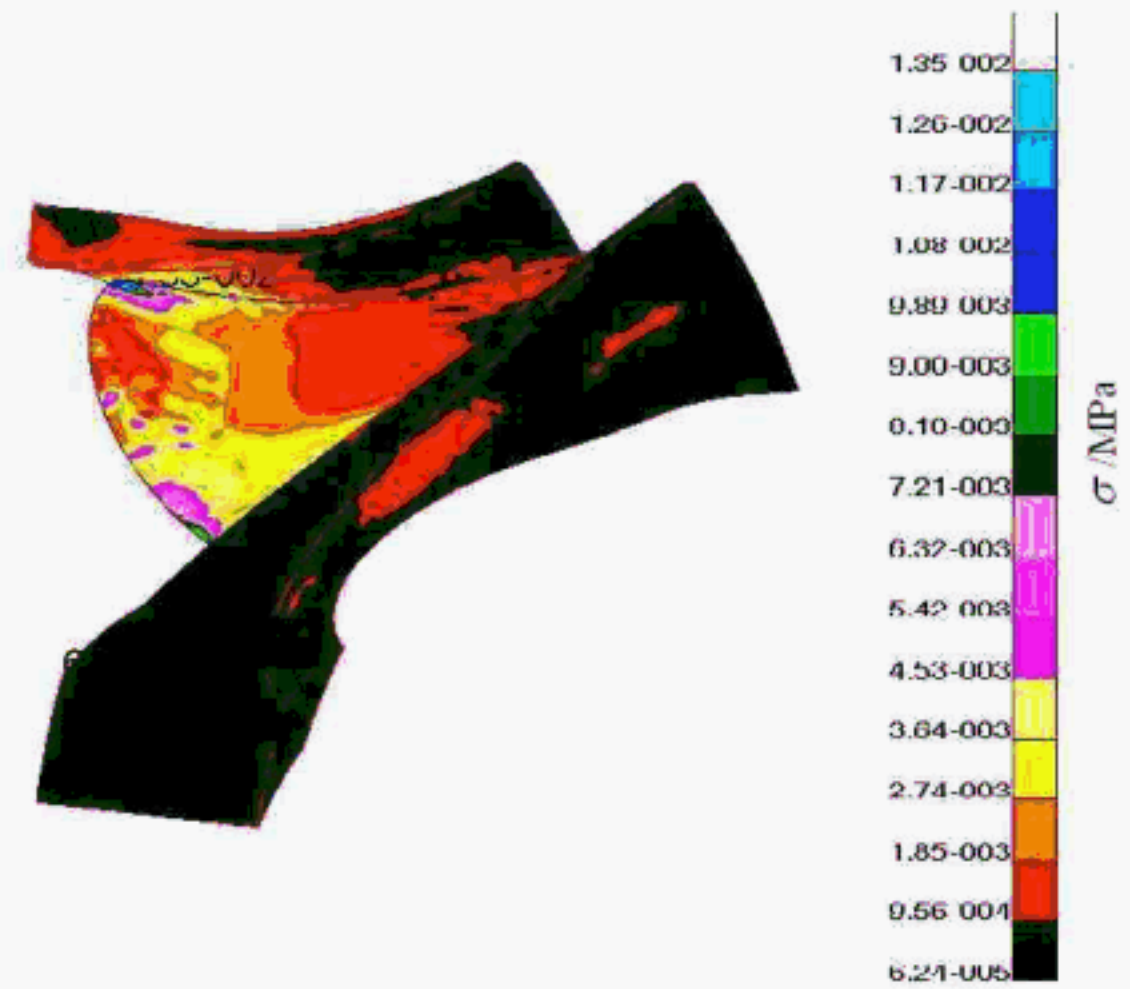


Figure 10. Alternating stress (1165Hz) on impeller blade

LIFETIME ESTIMATION

Using the weakly coupled FSI approach mentioned above, the amplitude σ_{kl} and phase φ_{kl} of the l th component of alternating stresses on the k th blade are obtained and then total alternating stress on each centrifugal impeller blade is calculated using the following formulation

$$\sigma = \sigma_c + \sum_{l=0}^h \left(\sum_{k=0}^{N-1} \sigma_{kl} e^{i(\varphi_{kl} + 2\pi k / Z_2)} \right) e^{i\omega t} \quad (4)$$

where σ_c is the static stress generated by centrifugal force, N is the number of impeller blades. From the equation (4), the averaged stress $\sigma_m = 634$ MPa and nominal dynamic stress $\Delta\sigma_n = 12$ MPa on impeller blades are obtained.

In order to convert the nominal dynamic stress $\Delta\sigma_n$ to local stress strain, the modified Neuber formulation is used

$$\Delta\sigma\Delta\varepsilon = K_f^2 \Delta\sigma_n^2 / E \quad (5)$$

and

$$\Delta\varepsilon = \Delta\sigma / E + 2(\Delta\sigma / K')^{1/n'} \quad (6)$$

Combining equations (5) and (6), the actual stress amplitude $\Delta\sigma = 14$ MPa and strain amplitude $\Delta\varepsilon = 1.5 \times 10^{-4}$ are computed using an iterative solving technique. And the lifetime

of the impeller blade is estimated using the modified Manson-Coffin formula considering the effect of average stress

$$\Delta \varepsilon = \frac{\sigma'_f - \sigma_m}{E} (2N)^b + \varepsilon'_f (2N)^c \quad (7)$$

where the values of parameters in equations (5)-(7) are

Young's modulus $E=2.1 \times 10^5$ MPa

Cyclic hardening exponent $n'=0.128$

Cyclic hardening exponent $K'=1056$ MPa

Fatigue ductility coefficient $\varepsilon'_f = -0.3801$

Fatigue strength coefficient $\sigma'_f = 632$ MPa

Fatigue strength exponent $b=0.0743$

Fatigue ductility exponent $c=-0.5791$

Effective stress concentrative coefficient $K_f=1.5$

From equation (7) the estimation value of the cyclic times $N=9.7759 \times 10^8$ is corresponding to 135.9 days. The work identifies the necessity for modal response combination to achieve a good correlation between calculated HCF life and actual HCF life achieved.

CONCLUSIONS

The fracture failure of centrifugal impeller blades is analyzed with the weakly coupled FSI approach, and the key conclusions of the investigation are summarized as follows.

1. Pressure fluctuation on the impeller blades is dominated by the potential and viscous wake flow interaction between IGV and impeller, the region of the strongest pressure fluctuation is near the leading edge of impeller blades.
2. The insufficient margin between the dominant frequency of pressure fluctuation and the 6th natural frequency of impeller blade results in a local resonance vibration at the leading edge of the impeller blades.
3. Although the equivalent alternating stress near the leading edge of the impeller blades it is much less than the yield stress, the HCF failure of the impeller blades is caused by the long-term excitation of unsteady alternating stress.
4. The predicted alternating stress concentration region on the impeller blades in accordance with the actual fracture position validates the weakly coupled FSI approach used in this paper.

ACKNOWLEDGMENTS

The authors would like to thank Dr. Li Songtao (Carrier China Corporation) for the valuable help and discussion during the preparation of the manuscript.

REFERENCES

- [1] He, P., Du D, M. 2005, "Research on life assessment and monitoring system of steam turbine", In Proceedings of the ASME Power Conference, Chicago, Apr, 5-7, 2005.

- [2] Rao, J. S., 1994, *Turbomachine unsteady aerodynamics*, New Age International, London, England.
- [3] Parrondo, J. L., Gonzalez, J., Fernandez, J., 2002, "The Effect of the Operating Point on the Pressure Fluctuations at the Blade Passing Frequency in the Volute of a Centrifugal Pump". *ASME Journal of Fluids Engineering*, Vol.124 (9), pp. 784-790.
- [4] Choi, J. S., McLaughlin, D. K., Thompson, D.E., 2003, "Experiments on the unsteady flow field and noise generation in a centrifugal pump impeller". *Journal of Sound and Vibration*, Vol. 26(3), pp. 493-514.
- [5] Feshe, K. R, Neise, W., 1999, "Generation Mechanisms of Low-Frequency Centrifugal Fan Noise", *AIAA Journal*, Vol. 37(10), pp. 1173-1179.
- [6] Sullivan, J. P., Gregory, J. W., 2002, "Unsteady pressure measurements in turbomachinery using porous pressure sensitive paint", In AIAA aerospace sciences meeting and exhibit, Reno, Jan, 14-17, 2002.
- [7] Dickmann, H. P., Wimmel, T. S., Szwedowicz, J. et al., 2006, "Unsteady flow in a turbocharger centrifugal compressor: Three-dimensional computational fluid dynamics simulation and numerical and experimental analysis of impeller blade vibration", *ASME Journal of Turbomachinery*, Vol. 128(3), pp. 455-465.
- [8] Hillewaert, K., Van den Braembussche, R., A., 1999, "Numerical simulation of impeller-volute interaction in centrifugal compressors", *ASME Journal of Turbomachinery*, Vol. 121(3), pp. 603-608.
- [9] Guleren, K. M., Turan, A., Pinarbasi A., 2008, "Large-eddy simulation of the flow in a low-speed centrifugal compressor", *International Journal for numerical methods in fluids*, Vol. 56(8), pp. 1271-1280.
- [10] Lee, S., Kim. H. J., Kim. J. H., 2003, "Computation of turbulent flows and radiated sound from axial compressor cascade using LES". In Proceedings of the ASME Fluids Engineering Division Summer Meeting, New Orleans, United States, pp.159-166.
- [11] Dowell, E. H., Hall, K. C., 2001, "Modeling of fluid-structure interaction", *Annual review of fluid mechanics*, Vol. 33, pp.445-490.
- [12] Barth, T.J., Griebel, M., Keyes, D.E., et al, 2006, *Fluid-structure interaction modeling, simulation, optimization*, Springer, London, England.
- [13] Carstens, V., Belz, J., 2001, "Numerical investigation of nonlinear fluid-structure interaction in vibrating compressor blades", *ASME Journal of Turbomachinery*, Vol. 123(2), pp. 402-408.
- [14] Carstens, V., Kemme, R., Schmitt, S., 2003, "Coupled simulation of flow structure interaction in turbomachinery", *Aerospace Science and Technology*, Vol. 7, pp. 298-306.
- [15] Dickmann, H. P. Wimmel, T. S., Szwedowicz, J., et al., 2006, "Unsteady flow in a turbocharger centrifugal compressor: three-dimensional computational fluid

- dynamics simulation and numerical and experimental analysis of impeller blade vibration”, *ASME Journal of Turbomachinery*, **Vol.** 128, pp. 455-465.
- [16] Filsinger, D., Szwedocicz, J., Schafer, O., 2002, “Approach to unidirectional coupled CFD-FEM analysis of axial turbocharger turbine blades”, *ASME Journal of Turbomachinery*, **Vol.** 124(1), pp. 125-131.
- [17] Misek, T., Tetiva, A., Prchlik, L., Duchek, K., 2007, “Prediction of high cycle fatigue life of steam turbine blading based on unsteady CFD and FEM forced response calculation”, In ASME Turbo Expo 2007, May 17-17, Montreal.
- [18] Srivastava, R., Lentz, J., Liu, J.S., Panovsky, J., 2007, “Computation of unsteady flowfield and blade response due to impeller-diffuser interaction”, In ASME Turbo Expo 2007, May 17-17, Montreal.
- [19] Srinivasan, A. V., Cutts, D. G., 1984, “Measurement of relative vibratory motion at the shroud interfaces of a fan”, *ASME Journal of Vibration of acoustic and stress, and reliability in design*, **Vol.**106, pp. 189-197.
- [20] Rao, J. S., Vyas, N. S., 1996, “Determination of blade stresses under constant speed and transient conditions with nonlinear damping”, *ASME Journal of Engineering for Gas Turbines and Power*, **Vol.** 118(2), pp.424-432
- [21] Kielb, J. J., Abhari, R. S., 2003, “Experimental study of aerodynamic and structural damping in a full-scale rotating turbine”, *ASME Journal of Engineering for Gas Turbines and Power*, **Vol.** 125(1), pp. 102-112.
- [22] Miner, M. A., 1945, “Cumulative damage in fatigue”, *ASME Journal of Applied mechanics*, **Vol.** 67, pp.159.
- [23] Corten, H. T., Dolan, T. J., 1956, “Cumulative fatigue damage”, In Proceeding of international conference on fatigue of metals, ASME and IME, pp.235.
- [24] Manson, S. S., Halford, G. R., 1981, “Practical implementation of the double linear damage rule and damage curve approach for treating cumulative fatigue damage”, *International Journal of Fracture*, **Vol.** 17(2):, pp. 169-192.
- [25] Niu, X., Li, G. X., Lee, H., 1987, “Hardening law and fatigue damage of a cyclic hardening metal”, *Engineering Fracture Mechanics*, **Vol.** 26(2), pp. 163-170.
- [26] Vyas, N. S., Rao, J. S., 1994, “Fatigue life estimation procedure for a turbine blade under transient loads”, *ASME Journal of Engineering for Gas Turbines and Power*, **Vol.** 116(1), pp.198-206.
- [27] Blevins, R. D., 1977, *Flow-induced vibration*, Van Nostrand Reinhold Company, New York.
- [28] Xu, Z. L., Park, J. P., Ryu, S. J., 2006, “Failure analysis and retrofit design of low pressure 1st stage blades for a steam turbine”, *Engineering Failure analysis*, **Vol.** 14, pp. 694-701.